Structure and thermodynamics of discrete potential fluids in the OZ–HMSA formalism

2007 J. Phys.: Condens. Matter 19 086224

(http://iopscience.iop.org/0953-8984/19/8/086224)

IOP PUBLISHING JOURNAL OF PHYSICS: CONDENSED MATTER

J. Phys.: Condens. Matter **19** (2007) 086224 (14pp) doi:10.1088/0953-8984/19/8/086224

Structure and thermodynamics of discrete potential fluids in the OZ–HMSA formalism

I Guillén-Escamilla[1], **M Chávez-Páez**[1] **and R Castañeda-Priego**[2]

[1] Instituto de Física, Universidad Autónoma de San Luis Potosí, Alvaro Obregón 64, 78000 San Luis Potosí, SLP, Mexico
[2] Instituto de Física, Universidad de Guanajuato, Loma del Bosque 103, Lomas del Campestre, 37150 León, Mexico

E-mail: mchavez@ifisica.uaslp.mx

Received 1 November 2006, in final form 29 December 2006
Published 9 February 2007
Online at stacks.iop.org/JPhysCM/19/086224

Abstract

We study the structural and thermodynamic properties of three discrete potential fluids: the square well (SW), the square well–barrier (SWB), and the square well–barrier–well (SWBW) fluids by means of the Ornstein–Zernike (OZ) integral equation and the HMSA (hybrid mean spherical approximation) closure relation. The radial distribution functions, structure factors, and pressure of the systems are calculated as a function of the strength of the attractive and repulsive parts of the potential in an extended range of densities, mainly covering the range $0.1 \leqslant \rho^* \leqslant 0.9$. We find that far away from the liquid–vapour coexistence region the HMSA theory is an accurate approach that compares well with Monte Carlo simulations. We also find that when the attractive parts of the potential dominate over the repulsive part the structure factor at low q values shows a considerable increase, which suggests the formation of large-scale domains that locally exhibit fluid-like structure.

1. Introduction

Structural and thermodynamic properties of both simple and complex fluids depend on the nature of the interaction potential between particles. While simple fluids can be modelled through a simple potential, in complex fluids one has often to resort to simplified schemes and introduce effective interactions between the main constituents of the fluid. In this process the effective potential is devised, from first principles or from experimental evidence, such that it captures enough features to reproduce the properties of the system it is supposed to model. Examples of such potentials are the Lennard-Jones and the DLVO potentials [1, 2]. The former describes very well the properties of many simple liquids and the latter is commonly used to describe the interaction between charged colloidal particles. Qualitatively, the DLVO potential is formed by a hard core followed by a short-range attractive well and a long-range repulsive barrier. For colloidal particles at interphases, the effective interaction can include a secondary

minimum [3]. The stability of colloidal systems depends crucially on the presence of such an energetic barrier, whereas the second attractive component modifies drastically the properties of the systems. In this work we use a simplified interaction model, a discrete potential (DP), that incorporates attractive and repulsive parts. Due to its simplicity, a DP allows us to study separately the effects produced by the different attractive and repulsive components of the potential, which typically cannot be done with continuous potentials, where only global effects can be distinguished.

During the last few decades, discrete potentials have been used as simple models to investigate properties of continuous potential systems. They have been used, for example, to model the interactions of colloids and protein solutions [4, 5]. Despite its simplicity, a DP fluid can exhibit rather complex and interesting behaviours. Recently, for instance, it has been established that such fluids exhibit both liquid–vapour and liquid–liquid transitions [6]. Discrete potentials have been incorporated in a variety of statistical mechanics theories such as thermodynamic perturbation-like theories to describe associating fluids and polar fluids [7, 8]. In addition, their bulk properties can be used as inputs in the study of model inhomogeneous systems, i.e. for fluids in external fields such as porous media or confined systems [9]. All these aspects make DP systems interesting to explore.

The simplest and most investigated DP system is the well known square-well (SW) fluid. This model system can reproduce the behaviour of a large variety of real fluids by only varying the interaction range of the SW potential. The structural properties, as well as the liquid–vapour (LV), solid, and glass transitions of the SW fluid, have been studied by means of computer simulations, perturbation theory, and integral equation theory [4, 10–28]. Recently, within the framework of the self-consistent Ornstein–Zernike approximation (SCOZA), its LV coexistence has been reinvestigated and described with high accuracy [29]; a similar study on the liquid–solid transition within the SCOZA approach is in progress [30]. Although it has been shown that SCOZA yields globally accurate structural and thermodynamic properties of SW fluids and other systems, even near phase transitions and in the critical region, it becomes unstable for systems with potentials that include a second repulsive part (the problem resides in the diffusion-like coefficient of the associated partial differential equation (PDE), equation (9) in [29], which becomes negative when a repulsive barrier is considered, severely limiting the convergence of the PDE). It is therefore desirable to investigate other theoretical approaches that can handle this kind of potentials. In this paper we investigate one of these approaches, namely, the Ornstein–Zernike (OZ) equation in the HMSA approach [31].

The aim of this paper is to investigate the structural and thermodynamic properties of discrete potential fluids using the OZ–HMSA formalism. In particular, we investigate three different discrete potential fluids: the square well (SW), square well–barrier (SWB), and square well–barrier–well (SWBW) fluids. We analyse their radial distribution functions and structure factors as a function of the density and the energetic strength of the wells and barriers. In particular we focus our study on systems outside the liquid–vapour coexistence region. The theoretical predictions are contrasted with Monte Carlo simulations performed in the canonical ensemble.

After the present introduction, in section 2 we provide a detailed description of the discrete potentials, the theoretical approach, and the simulation method. In section 3 the structure functions and the pressure far away from the binodal are analysed. Finally, in section 4 we close the paper with a section of remarks and conclusions.

2. Model system and theoretical approach

Our system is formed by spherical particles of bulk density ρ and hard-core diameter σ in thermal equilibrium with a heat bath at absolute temperature T. The particles in this fluid

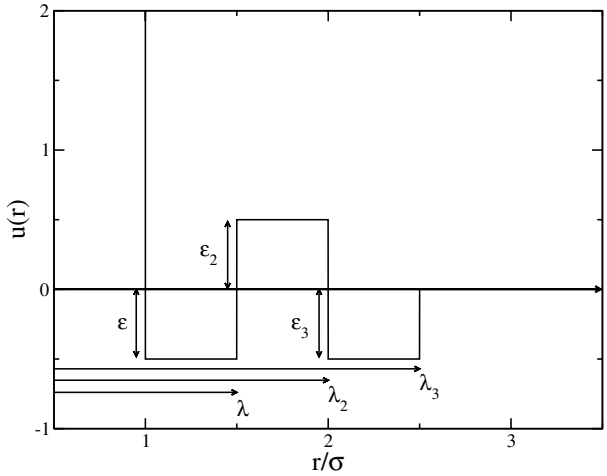

Figure 1. Cartoon of the discrete potential used in this work.

interact through a discrete potential that sequentially includes a hard sphere, a square well, a square barrier, and a second square well. This pair potential takes the form

$$u(r) = \begin{cases} \infty, & r < \sigma; \\ -\epsilon, & \sigma \leqslant r < \lambda\sigma; \\ \epsilon_2, & \lambda\sigma \leqslant r < \lambda_2\sigma; \\ -\epsilon_3, & \lambda_2\sigma \leqslant r < \lambda_3\sigma; \\ 0, & r \geqslant \lambda_3\sigma. \end{cases} \tag{1}$$

The parameters λ, λ_2, and λ_3 define the discontinuity points of the potential, and delimit the different regions of the potential. The parameters ϵ, ϵ_2, and ϵ_3, on the other hand, characterize the strength of the potential in those regions. A cartoon of the potential is presented in figure 1. Appropriate reduced quantities can be defined by scaling with the energy depth ϵ and the size of the particles σ, which leads to the reduced density $\rho^* = \rho\sigma^3$ and the reduced temperature $T^* = k_B T/\epsilon$, where k_B is the Boltzmann's constant. From equation (1) several cases can be considered, depending on the parameters; in particular, equation (1) reduces to the hard-sphere (HS) potential when only the first part is considered. We will consider the three following cases of equation (1): (a) the SW potential, defined by $\epsilon \neq 0$ and $\epsilon_2 = \epsilon_3 = 0$; (b) the SWB potential, defined by $\epsilon \neq 0$, $\epsilon_2 \neq 0$, and $\epsilon_3 = 0$; and (c) the SWBW potential, defined by the full equation (1). In this way, SW fluids are characterized by a single well, SWB fluids by a well and a barrier, and SWB fluids by two wells with a barrier in between.

From a theoretical point of view, we have selected the Ornstein–Zernike equation complemented with HMSA, a closure proposed by Zerah and Hansen that combines the hypernetted chain (HNC) and the soft mean spherical approximation (SMSA) [31]. This is a theoretical approach that has been applied with success in a large variety of simple and complex systems with both attractive and repulsive interactions [32–37]. However, its applicability to DP systems has not been explored yet. We also use the so-called mean spherical approximation (MSA), which has been used to study several kinds of simple fluids, in particular the SW fluid, but it has not been used to study SWB and SWBW fluids. Although other closure relations like Percus–Yevick (PY) could be used [11, 33, 38], here we shall focus only on the HMSA and MSA closures.

The homogeneous OZ equation is given by [39]

$$h(r) = c(r) + \rho \int h(|\mathbf{r} - \mathbf{r}'|)c(\mathbf{r}')\,\mathrm{d}\mathbf{r}', \tag{2}$$

where $h(r) = g(r) - 1$ and $c(r)$ are the total and direct correlation functions, respectively, and $g(r)$ is the radial pair distribution function. Alternatively, the OZ equation can be written in terms of the indirect correlation function $\gamma(r) = h(r) - c(r)$ by eliminating $h(r)$ from equation (2). In this work, the OZ equation is numerically solved by using a five-parameter version of the Ng iterative method [40]. Since the OZ equation defines $c(r)$ in terms of $h(r)$, an additional relation between $c(r)$ and $h(r)$ (or $\gamma(r)$) has to be provided to close the system. Many closure relations can be found in the literature of simple fluids and colloidal suspensions. The simplest one is the mean spherical approximation, which can be written as

$$c(r) = \begin{cases} -\gamma(r) - 1, & r < \sigma; \\ -\beta u(r), & r \geqslant \sigma, \end{cases} \tag{3}$$

where $\beta = 1/k_{\mathrm{B}}T$ is the inverse of the thermal energy. On the other hand, the HMSA closure relation can be written as [31]

$$c(r) = \exp\left[-\beta u_{\mathrm{r}}(r)\right]\left[1 + \frac{\exp\left[(\gamma(r) - \beta u_{\mathrm{a}}(r))f(r)\right] - 1}{f(r)}\right] - \gamma(r) - 1 \tag{4}$$

for $r \geqslant \sigma$, supplemented by the exact hard-sphere condition $c(r) = -\gamma(r) - 1$ for $r < \sigma$. In this equation, the total potential $u(r)$ between particles is split into two parts according to the HMSA recipe: $u_{\mathrm{r}}(r)$ is the repulsive part of the potential, and $u_{\mathrm{a}}(r)$ is the attractive part. The function $f(r) = 1 - \exp(-\alpha r)$ is a mixing function and α the mixing parameter. The isothermal compressibility χ of the system (normalized with the ideal gas compressibility $\chi_0 = \beta/\rho$) can be obtained through the relations $\chi_v^{-1} = (\partial\beta P/\partial\rho)_T$ (the virial route) and by $\chi_{\mathrm{c}}^{-1} = 1 - \rho\tilde{c}(q = 0)$, where P is the pressure of the system and $\tilde{c}(q)$ is the Fourier transform of the direct correlation function. The OZ–HMSA approach enforces both routes to give the same compressibility ($\chi_v = \chi_{\mathrm{c}}$) by adjusting the mixing parameter, imposing therefore partial thermodynamic consistency. The HMSA closure relation is an extension of an original relation proposed by Rogers and Young (RY) [41]. Although the RY relation works very well for systems with pure repulsive interactions, its applicability to systems with attractive interactions is rather restricted [31, 42], which led Zerah and Hansen to develop their closure relation.

Once the OZ equation has been solved, the pressure P of the system can be determined from the virial equation, which for the potential in equation (1) takes the form

$$\frac{\beta P}{\rho} = 1 + \frac{2}{3}\pi\rho\sigma^3\left[\sum_{i=0}^{3}\lambda_i^3\Delta g(\lambda_i)\right], \tag{5}$$

where λ_i denotes the discontinuity points of the potential, and $\Delta g(\lambda_i) = g(\lambda_i^+) - g(\lambda_i^-)$ is the difference in contact values of the radial distribution function at the discontinuity. For a HS fluid $i = 0$ and the summation only involves the term $\Delta g(\sigma) = g(\sigma^+)$. The SW fluid additionally involves $\Delta g(\lambda) = g(\lambda^+) - g(\lambda^-)$, the SWB involves also the term $\Delta g(\lambda_2) = g(\lambda_2^+) - g(\lambda_2^-)$, and finally the SWBW includes the contribution $\Delta g(\lambda_3) = g(\lambda_3^+) - g(\lambda_3^-)$.

The theoretical calculations are compared to Monte Carlo simulations in the canonical (NVT) ensemble [43, 44]. In all our simulations we used periodic boundary conditions, with a minimum of $N = 1024$ particles and a minimum simulation box length $L = 10\sigma$, depending on the density of the systems. The particles in the simulation box are initially placed in a regular configuration at the prescribed density; this configuration is equilibrated for at least 10^5 Monte Carlo cycles, where each MC cycle consist of N attempts to displace randomly selected

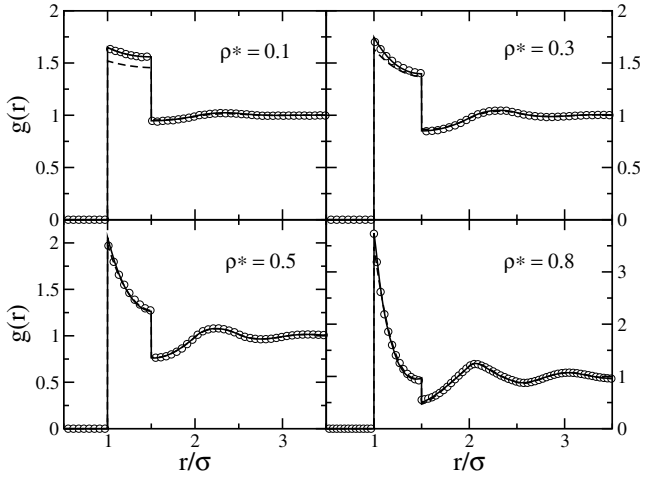

Figure 2. Radial distribution functions for system I, as obtained from HMSA (solid lines), MSA (dashed lines), and MC simulations (symbols).

Table 1. Systems studied in this work. The scaling units are ϵ and σ, which define the reduced temperature $T^* = k_B T/\epsilon$, the reduced energies $\epsilon_2^* = \epsilon_2/\epsilon$ and $\epsilon_3^* = \epsilon_3/\epsilon$, and the reduced density $\rho^* = \rho\sigma^3$.

System	Type	T^*	ϵ_2^*	ϵ_3^*	λ	λ_2	λ_3	T_c^*	ρ_c^*
I	SW	2.0	0.0	0.0	1.5	0.0	0.0	1.226	0.304
II	SWB	2.0	0.2	0.0	1.5	2.0	0.0	0.972	0.306
III	SWB	2.0	0.4	0.0	1.5	2.0	0.0	0.760	0.297
IV	SWBW	2.0	0.2	0.2	1.5	2.0	2.5	1.344	0.312

particles. After equilibration, at least 10^5 MC cycles are performed to determine the radial distribution functions. For our study we use several values of the density, mostly in the range $0.1 \leqslant \rho^* \leqslant 0.9$, keeping constant the interaction ranges $\lambda = 1.5$, $\lambda_2 = 2.0$, and $\lambda_3 = 2.5$. In particular, four systems are considered, as summarized in table 1. As shown in this table, only one reduced temperature is considered, namely, $T^* = 2.0$, which is above the critical temperature T_c of the systems, and therefore the systems are far away from the binodal line. The critical temperatures of the systems along with the corresponding critical densities ρ_c are shown in table 1. These critical points and the corresponding liquid–vapour phase diagrams were obtained by using Gibbs ensemble Monte Carlo simulations [45, 46] and will be reported elsewhere [9]. For system I, the liquid-phase diagram is reported in [29].

3. Results

3.1. SW fluids

We start our study with the SW fluid labelled as system I in table 1. For this system we calculated the structure for several densities, covering the range $0.1 \leqslant \rho^* \leqslant 0.9$, which covers from dilute to highly concentrated systems. In figure 2 we show HMSA, MSA, and MC radial distribution functions (RDFs) for the selected densities $\rho^* = 0.1, 0.3, 0.5, 0.8$. From the figure we can appreciate that the structure predicted by HMSA agrees very well with the simulation

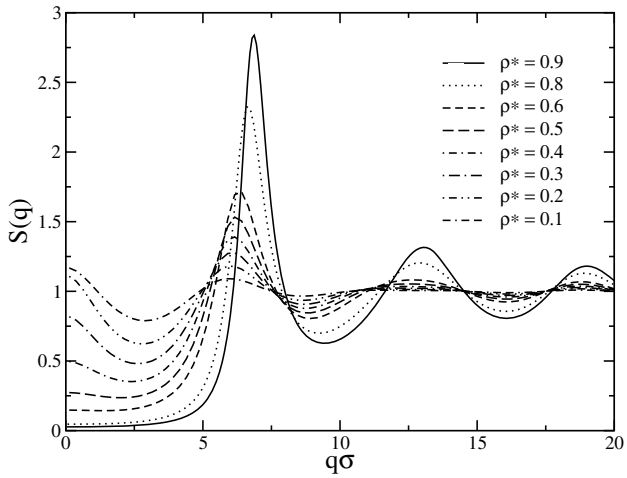

Figure 3. Structure factor of SW fluids (system I) for several reduced densities, as obtained from HMSA.

data and with previous reference hypernetted-chain (RHNC) calculations [47]. MSA, on the other hand, fails to reproduce the structure in the region of the attractive well for low densities, but the agreement improves greatly for $\rho^* \geqslant 0.4$. From the figure it can be seen that, as expected, the structure is enhanced when the density is increased. We note, however, that for all densities the agreement of HMSA and MSA with simulations is very good beyond the well of the potential. It is in the region of the well of the potential where discrepancies between the two theories are revealed.

The radial distribution function $g(r)$ is directly connected to the so-called structure factor $S(q)$ through the relation $S(q) = 1 + \rho\tilde{h}(q)$, where $\tilde{h}(q)$ is the Fourier transform of the total correlation function [39]. The structure factor describes the isothermal compressibility of the system since $S(q = 0) = \chi_c$ [39], as can be easily checked from the definition of both $S(q)$ and χ_c. $S(q)$ also gives structural information in the Fourier space and allows us to determine the main length scales present in the system. For SW fluids three length scales determine the structure, namely, the size of the particles σ, the range of the SW potential $\lambda\sigma$, and the mean distance between particles d_m, which is defined as $d_m = \rho^{-1/3}$. In figure 3 we show the structure factors of the SW fluid for several densities, as calculated by using HMSA; MSA results are not included to avoid an overloaded figure. For large wavevectors ($q\sigma > 2\pi/d_m^*$) the structure factor $S(q)$ exhibits a main peak located at $q\sigma \approx 2\pi$, which means that an important length scale of the SW fluid is the diameter of the particles. As the density of the system increases this peak increases and shifts slightly to larger wavevectors, which reflects the increasing correlations between the particles in the fluid.

The behaviour of $S(q)$ at small wavevectors is interesting. Since $S(q = 0) = \chi_c$ and $S(q = 0)$ decreases when the density of the system increases, this means that the compressibility of the system decreases. For low densities we observe that $S(q = 0) > 1$, which means that the compressibility of the SW fluid is larger than its ideal gas counterpart. On the other hand, we notice that the structure factor develops a distinct peak around $q = 0$ for densities $\rho^* < 0.4$. For low enough densities (for example $\rho^* = 0.1$), this peak is of similar or larger height than that of the principal peak of $S(q)$ located at $q\sigma \approx 2\pi$. This indicates that at low densities the system develops another important length scale that is much larger than the diameter of the particles or the mean distance between particles. This suggests

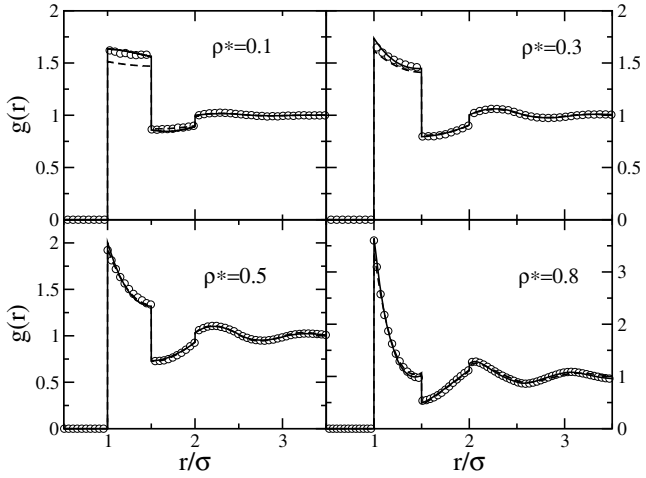

Figure 4. Radial distribution functions for system II, as obtained from HMSA (solid lines), MSA (dashed lines), and MC simulations (symbols).

that at small densities the attractive well induces the formation of domains whose size is much larger than the diameter of the particles; the local structure of these domains, however, would be liquid-like, as indicated by the behaviour of the corresponding radial distribution functions and structure factors shown in figures 2 and 3. Recently, similar trends have been observed in model colloidal suspensions and protein solutions with attractive interactions [48, 49].

Included in figure 3 is the structure factor for $\rho^* = 0.9$. For this density the height of the main peak is slightly above the critical value $S_c = 2.85$, where S_c signals the solidification of the system, according to the Hansen–Verlet criterion [50]. Thus, according to HMSA the SW fluid reaches the solid phase close to this density, which is smaller than the corresponding density of hard-sphere fluids ($\rho^* = 0.935$). Note, however, that the radial structure of the SW system is liquid-like because the underlying theoretical framework describes correlations in the fluid phase.

3.2. SWB fluids

For SWB fluids the pair potential includes one square well and one square barrier. Each part of the potential plays a role in the structure of the fluid, and many combinations are possible for the relative strength of the well and the barrier. Here we only consider two cases, namely, system II and system III presented in table 1. These two systems differ by the height of the barrier. In one case $\epsilon_2^* = 0.2$ and in the other $\epsilon_2^* = 0.4$; in both cases $\lambda = 1.5$, $\lambda_2 = 2.0$, and $T^* = k_B T/\epsilon = 2.0$. Figures 4 and 5 show HMSA, MSA, and MC RDFs for the selected densities $\rho^* = 0.1, 0.3, 0.5, 0.8$. For $\epsilon_2^* = 0.2$ the structure of the fluid predicted by the HMSA approach compares very well to the simulation data throughout the range of densities, especially at low densities, where the simulation–theory agreement is excellent. This agreement deteriorates slightly for very high densities ($\rho^* > 0.8$). For a higher barrier, as illustrated in figure 5 for $\epsilon_2^* = 0.4$, the overall simulation–theory agreement is still good, especially at low densities. Although the contact values are in general well reproduced, HMSA slightly overestimates the main contact value for $\rho^* > 0.5$. We find that for larger values of ϵ_2^* the simulation–theory agreement increasingly deteriorates (data not shown), especially the contact values, although the main features of the radial distribution functions are captured by the HMSA

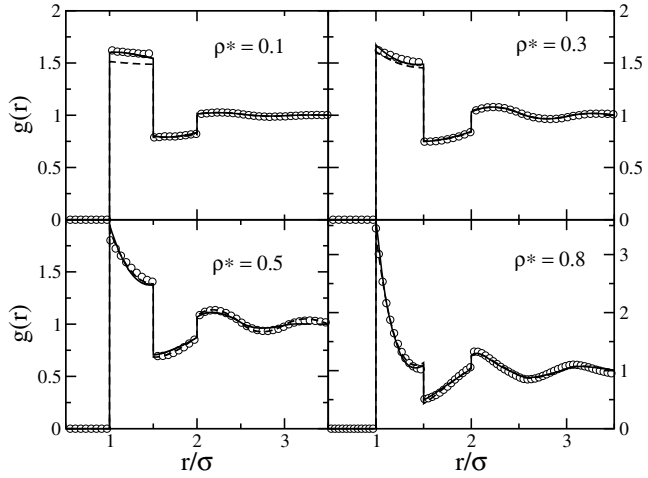

Figure 5. Radial distribution functions for system III, as obtained from HMSA (solid lines), MSA (dashed lines), and MC simulations (symbols).

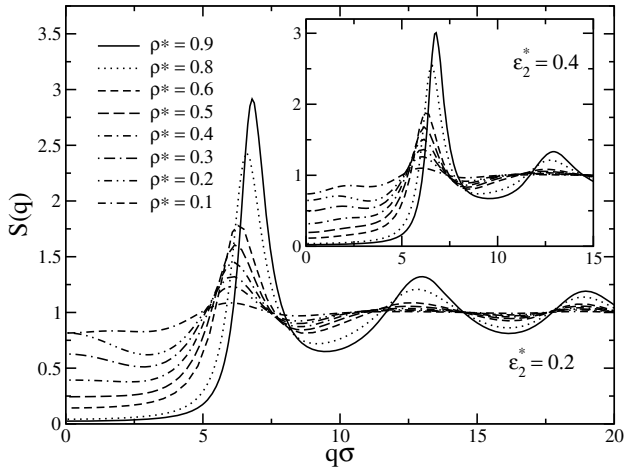

Figure 6. Structure factor of SWB fluids for several densities, as obtained from HMSA. In the main figure, $\epsilon_2^* = 0.2$ (system II). In the inset, $\epsilon_2^* = 0.4$ (system III).

theory. The performance of the MSA theory for SWB fluids, on the other hand, follows the same trends as already observed for SW fluids; for small densities it deviates from the MC data in the region of the well, but its performance improves as the density increases.

Structure factors for SWB fluids are shown in figure 6, covering the density range $0.1 \leqslant \rho^* \leqslant 0.9$. In the main body of the figure are shown systems with $\epsilon_2^* = 0.2$. For large wavevectors ($q\sigma > 2\pi/d_{\mathrm{m}}^*$) the structure factors follow the same trends as presented in figure 3. The dominant length scale of the systems is the size of the particles, since the position of the main peak is located around $q\sigma \approx 2\pi$. The heights of the peaks are, however, higher for SWB fluids than for SW fluids. This is clearly an effect induced by the presence of the repulsive barrier, which increases the correlations between the particles and induces more local order at short distance. As a result, SWB fluids reach the solid transition (according to the

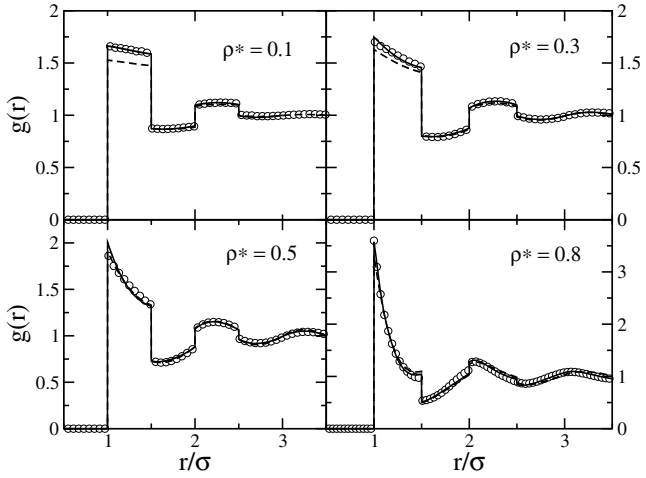

Figure 7. Radial distribution functions for system IV, as obtained from HMSA (solid lines), MSA (dashed lines), and MC (symbols).

Hansen–Verlet criterion) faster than SW fluids, as can be observed from the comparison of the main peaks of $S(q)$ at $\rho^* = 0.9$ for both SW and SWB fluids. This re-entry of the fluid–solid transition is similar to that observed in crystal and glass transitions of SW fluids [25–27], where it has been shown that the repulsive part of the potential (which tends to disperse the particles of the fluid) and the attractive part (which tends to reduce the average distance between particles) compete strongly and modulate in a non-trivial way the structure of the fluid. From the figure we see that the presence of the barrier also modifies the low-q behaviour of $S(q)$. In general the behaviour of $S(q = 0)$ shows that SWB systems are less compressible than SW systems. Although the structure factor at $q = 0$ develops a peak for small densities, it is always smaller than that of the main peak. This indicates that the inclusion of the barrier tends to prevent order at large scales, inhibiting the formation of large-scale domains.

The trends just described in the previous paragraph are more notorious for larger values of the barrier, as illustrated in the inset of figure 6, where the structure factors for $\epsilon_2^* = 0.4$ are presented. In fact, as can be seen by comparing the data in the inset with the corresponding data in the main body of the figure, the height of the main peak increases with the strength of the potential. This is a clear indication that the barrier induces stronger correlations and ordering in the systems. In fact, for $\epsilon_2^* = 0.4$ there appears another peak in the structure factor at $q\sigma \approx 2\pi/\lambda_2$. This peak, although weak, appears for low values of the density and disappears at high densities. The appearance of this peak indicates that another length scale, namely, $\lambda_2\sigma$, starts to dominate the structure of the systems. This is expected since in the limit of infinite barrier the SWB systems become systems of hard spheres of diameter $\lambda_2\sigma$. We note that the trends observed here are consistent with those reported in [51–53] for similar systems, where a repulsive barrier is employed to stabilize the liquid branch of the systems, suppressing liquid–gas separation.

3.3. SWBW fluids

In figure 7 we show the radial distribution functions for system IV in table 1. This system corresponds to an SWBW fluid at reduced temperature $T^* = k_B T/\epsilon = 2.0$ and pair potential parameters $\epsilon_2^* = 0.2$, $\epsilon_3^* = 0.2$, $\lambda = 1.5$, $\lambda_2 = 2.0$, and $\lambda_3 = 2.5$. The figure shows HMSA,

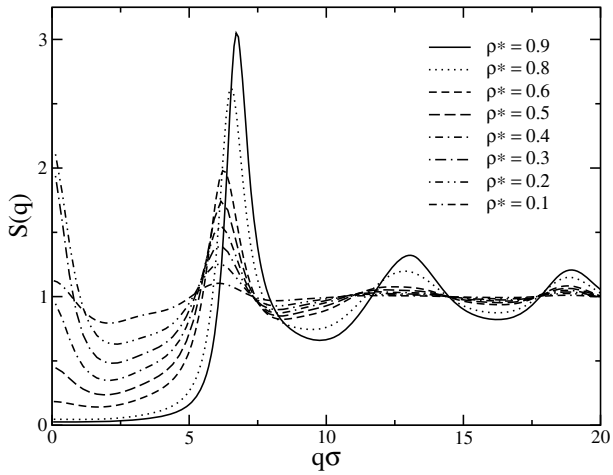

Figure 8. Structure factor of SWBW fluids (system IV) for several densities, as obtained from HMSA.

MSA, and MC data for the selected densities $\rho^* = 0.1, 0.3, 0.5, 0.8$. Overall, the comparison between HMSA and MC data is very good, especially at low and intermediate densities. For $\rho^* \geqslant 0.6$, however, it can be seen that HMSA does not reproduce well the contact values predicted by MC, especially the main contact values; the rest of the structure is well reproduced. The performance of MSA, on the other hand, follows the same trends as already observed for SW and SWB fluids.

The structure factor of SWBW systems is shown in figure 8. It is clear from the figure that the local order and the compressibility are strongly affected by the presence of the second attractive well. On the one hand, there is an increase in the local order for large wavevectors, as evidenced by the high peaks of the structure factor around the wavevector $q\sigma = 2\pi$; on the other hand, there is a dramatic increase in the compressibility and long-range order (i.e. very low q vectors) for low densities. This effect disappears at high densities due to the entropic contributions since the excluded volume interactions dominate the structure at these densities. In SW fluids we found that the attractive part of the potential induced this long-range order; in SWBW fluids, however, it is the combination of the barrier and the wells that induce this order, since in this case the effective range of the attractive interactions is increased. In any case, the addition of a secondary attractive part to the potential seems to induce strong correlations both at short and large particle separations, the last one indicating the possible formation of domains at low densities. Interestingly, we observe that for $\rho^* = 0.1$ the low-q behaviour has reversed its trend, drastically decreasing the long-range order and compressibility of the system. This effect arises because for this density most of the particles are separated by the mean distance $d_{\mathrm{m}}^* \approx 2.15$, i.e. beyond the direct influence of the barrier ($\lambda_2 = 2.0$), but in the region of the second attractive well. These particles therefore have to surmount an unfavourable barrier $\Delta\epsilon = \epsilon_2 + \epsilon_3$ to get closer. This same effect, although weak, can be observed already in figure 6.

3.4. RDF contact values and pressure

In sections 3.1–3.3 we presented results for the radial distributions and structure factors of discrete potential fluids. We found that the overall structure predicted by HMSA compares

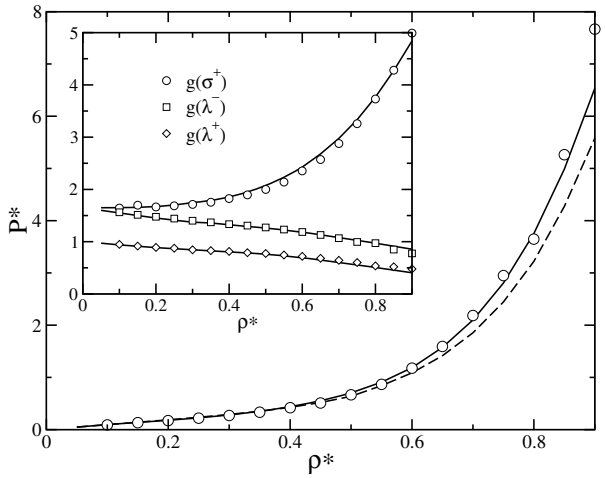

Figure 9. Reduced pressure $P^* = \beta P/\rho$ of SW fluids (system I) as a function of density. Solid lines correspond to HMSA, dashed lines to MSA, and symbols to MC. In the inset, HMSA and MC contact values as a function of density.

well with Monte Carlo simulation data. However, another comparison between theory and simulations can be done at the level of the thermodynamic pressure of the systems. Since the pressure of DP fluids depends on the contact values of the RDF (see equation (5)), it is important to predict accurately the contact values. In this section we present comparisons between HMSA and Monte Carlo for the pressure and contact values of the radial distribution functions for the systems described in table 1.

Figure 9 shows the pressure of the SW fluids studied previously for HMSA (solid line), MSA (dashed line), and MC (symbols). The HMSA results are in very good agreement with the simulation data up to very high densities. The only point in the curve that is not well reproduced by the HMSA theory corresponds to $\rho^* = 0.9$. The good theory–simulation agreement observed in the figure is the consequence of a good prediction of the contact values of the radial distribution functions at the discontinuities of the potential, as illustrated in the inset of the figure. In this inset we present results for the HMSA and MC contact values $g(\sigma^+)$, $g(\lambda^-)$, and $g(\lambda^+)$ as a function of the density of the fluid. Here we see that all the contact values are well predicted. The mayor deviations are observed at $\rho^* = 0.9$, which leads to the underestimation of the theoretical pressure observed in the figure. We note that the contact value $g(\sigma^+)$ is a strongly increasing function of the density, which is the typical behaviour of hard-sphere fluids. The other contact values decrease with density. Since $\Delta g(\lambda)$ decreases slightly, the strong increase of the pressure as a function of density is dominated by the contributions of the main contact value.

Figure 10 shows the pressure of SWB fluids with interaction parameter $\epsilon_2^* = 0.4$. Both theory and simulations are included. The behaviour here is similar to that observed in the previous figure. In this case, however, HMSA deviates from the simulation data for $\rho^* > 0.75$. This is due to the inability of the theory to predict correctly the contributions of the several contact values of the radial distribution function at high densities. In contrast to the SW case where only three contact values contribute to the pressure, for SWB fluids five contact values have to be predicted accurately to maintain good theory–simulation agreement. The inset of the figure shows, for $\epsilon_2^* = 0.4$, the contact values predicted by HMSA and those obtained by simulations. From this inset we see that the main contact value increases with density,

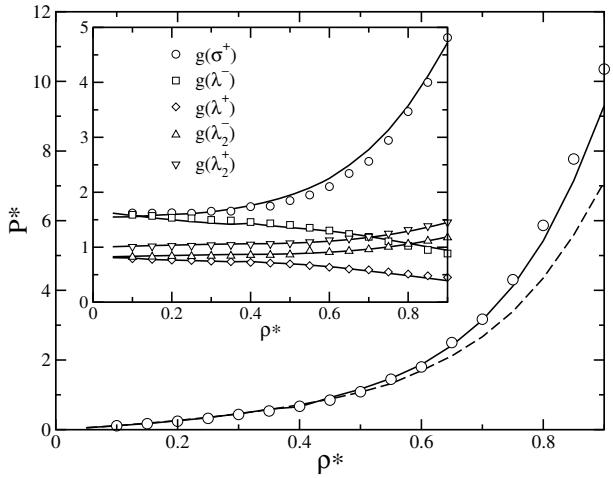

Figure 10. Reduced pressure $P^* = \beta P/\rho$ of SWB fluids as a function of density for $\epsilon_2^* = 0.4$ (system III). Solid lines correspond to HMSA, dashed lines to MSA, and symbols to MC. In the inset, HMSA and MC contact values as a function of density.

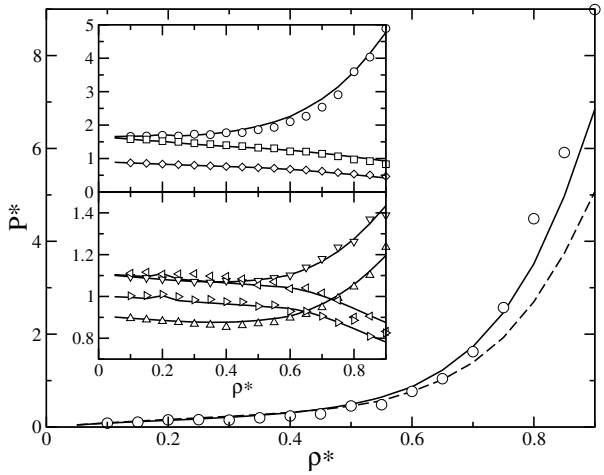

Figure 11. Reduced pressure $P^* = \beta P/\rho$ of SWBW fluids (system IV) as a function of density. Solid lines correspond to HMSA, dashed lines to MSA, and symbols to MC. In the insets, HMSA and MC contact values as a function of density. In the top inset, $g(\sigma+)$ (circles), $g(\lambda^-)$ (squares), and $g(\lambda^+)$ (diamonds). In the bottom inset, $g(\lambda_2^-)$ (down triangle), $g(\lambda_2^+)$ (up triangle), $g(\lambda_3^-)$ (left triangle), and $g(\lambda_3^+)$ (right triangle).

with good theory–simulation agreement, except at moderate densities. The contact values at $r = \lambda\sigma$, on the other hand, decrease with density, with good theory–simulation agreement except at high densities. For $r = \lambda_2\sigma$ the contact values increase with density, the agreement with simulations is good, and the difference $\Delta g(\lambda_2)$ is small. Thus, the theory–simulation discrepancies at $r = \sigma$ and $r = \lambda\sigma$ account for the theory–simulation deviations observed in the pressure.

The pressure for SWBW fluids is shown in figure 11. In this case, the HMSA gives a good estimation of the pressure at low densities, slightly overestimates it at moderate densities,

and underestimates it at higher densities. Overall, the agreement with simulations is good for densities up to $\rho^* \approx 0.75$. Beyond this density the discrepancies are important. The comparison between HMSA and MC contact values is presented in the two insets. The top inset shows the contact values at $r = \sigma$ and $\lambda\sigma$, and the bottom inset at $r = \lambda_2\sigma$ and $\lambda_3\sigma$. The behaviour of the contact values is clearly seen in these insets: the contact values at $r = \sigma$ and $\lambda_2\sigma$ (which define the repulsive parts of the potential) increase with density, whereas the contact values at $\lambda\sigma$ and $\lambda_3\sigma$ (which define the attractive parts of the potential) decrease with density. All these trends are confirmed by the simulations. From the comparisons in the insets we see that the main contact value predicted by HMSA agrees well with simulations for low densities, but overestimates it at intermediate densities, which is reflected in the corresponding comparison of the pressure. At high densities the secondary contact values show discrepancies with simulation. These discrepancies lead to the theoretical underestimation of the pressure observed in the figure.

MSA results for the pressure are also included in figures 9–11. As shown in these figures, MSA predicts very well the pressure of the systems up to densities $\rho^* \approx 0.5$. For larger densities MSA clearly deviates from the MC and HMSA data, underestimating the pressure systematically as the density increases.

4. Summary

In this work, we have studied both structural and thermodynamic properties of discrete potential fluids by using the Ornstein–Zernike equation together with the HMSA closure relation. The results were compared with the mean spherical approximation theory and with NVT Monte Carlo computer simulations. We found that far away from the coexistence region HMSA provides an accurate description of the system properties, and that HMSA is a better approach than MSA.

We also found that, in the regime of applicability of HMSA, the inclusion of attractive and repulsive components in the potential promotes dramatic changes in the local and long-range order of the systems. We observed that the attractive components induce higher compressibility and the possible formation of clusters or domains, which locally show a fluid-like structure. On the other hand, the repulsive part of the potential tends to stabilize the systems, inhibiting the formation of these domains and lowering the compressibility. Also, we found that, in general, the (virial) equation of state provided by the HMSA relation describes well the pressure of the systems.

Finally, we conclude that this work allows us to identify regions of applicability of the HMSA closure relation when it is applied to simple fluids with both attractive wells and repulsive barriers. This information becomes useful for inhomogeneous systems or dynamic theories where accurate knowledge of the bulk properties is required [4, 25, 27, 51, 52, 54–56].

Acknowledgments

We acknowledge financial support from CONACYT, Mexico, grants 46373/A-1, J37530E and U47611-F, and PROMEP (SEP, Mexico).

References

[1] Barker J A and Henderson D 1976 *Rev. Mod. Phys.* **48** 587
[2] Derjaguin B V and Johnston R K 1989 *Theory of Stability of Colloids and Thin Films* (New York: Consultants Bureau)
[3] Ruiz-García J, Gámez-Corrales J R and Ivlev B I 1998 *Mol. Phys.* **95** 371

[4] Bergenholtz J and Fuchs M 1999 *Phys. Rev.* E **59** 5706
[5] Lutsko J F and Nicolis G 2005 *J. Chem. Phys.* **122** 244907
[6] Malescio G, Franzese G, Pellicane G, Skibinsky A, Buldyrev S V and Stanley H E 2002 *J. Phys.: Condens. Matter* **14** 2193
[7] Benavides A L and Gil-Villegas A 1999 *Mol. Phys.* **97** 1225
[8] Vidales A, Benavides A L and Gil-Villegas A 2001 *Mol. Phys.* **99** 703
[9] Guillén-Escamilla I and Chávez-Páez M 2007 at press
[10] Baxter R J 1968 *J. Chem. Phys.* **49** 2770
[11] Smith W R, Henderson D and Barker J A 1971 *J. Chem. Phys.* **55** 4027
[12] Henderson D, Barker J A and Smith W R 1976 *J. Chem. Phys.* **64** 4244
[13] Nezbeda I 1977 *Czech. J. Phys.* B **27** 247
[14] Benavides A L and Gil-Villegas A 1999 *Mol. Phys.* **97** 1225
[15] Henderson D, Scalise O H and Smith W R 1980 *J. Chem. Phys.* **72** 2431
[16] Largo J, Solana J R, Yuste S B and Santos A 2005 *J. Chem. Phys.* **122** 084510
[17] Smith W R and Henderson D 1978 *J. Chem. Phys.* **69** 319
[18] Smith W R, Henderson D and Tago Y 1977 *J. Chem. Phys.* **67** 5308
[19] Henderson D, Maden W G and Fitts D D 1976 *J. Chem. Phys.* **64** 5026
[20] Tago Y 1974 *J. Chem. Phys.* **60** 1531
[21] Largo J, Solana J R and Santos A 2003 *Mol. Phys.* **101** 2981
[22] Davies L A, Gil-Villegas A and Jackson G 1999 *J. Chem. Phys.* **111** 8659
[23] Smith W R, Henderson D and Murphy R D 1974 *J. Chem. Phys.* **61** 2911
[24] Alder G J, Young D A and Mark M A 1980 *J. Chem. Phys.* **56** 3013
[25] Dawson K, Foffi F, Fuchs M, Götze W, Sciortino F, Sperl M, Tartaglia P, Voigtmann Th and Zaccarelli E 2000 *Phys. Rev.* E **63** 11401
[26] Bolhuis P, Hagen M and Frenkel D 1994 *Phys. Rev.* E **50** 4880
[27] Fabbian L, Götze W, Sciortino F, Tartaglia P and Thiery F 1999 *Phys. Rev.* E **59** R1347
[28] Foffi G, McCullagh G D, Lawlor A, Zaccarelli E, Dawson K, Sciortino F, Tartaglia P, Pini D and Stell G 2002 *Phys. Rev.* E **65** 031407
[29] Schöll-Paschinger E, Benavides A L and Castañeda-Priego R 2005 *J. Chem. Phys.* **123** 234513
[30] Benavides A L 2006 private communication
[31] Zerah G and Hansen J P 1986 *J. Chem. Phys.* **84** 2336
[32] Caccamo C, Giaquinta P V and Giunta G 1993 *J. Phys.: Condens. Matter* **5** B75
[33] Caccamo C 1996 *Phys. Rep.* **274** 1
[34] González-Mozuelos P and Carbajal-Tinoco M D 1998 *J. Chem. Phys.* **109** 11074
[35] Coluzzi B, Parisi G and Verrochio P 2000 *Phys. Rev. Lett.* **84** 306
[36] Pastore G, Santin R, Taraphder S and Colonna F 2005 *J. Chem. Phys.* **122** 181104
[37] Kunor T R and Taraphder S 2006 *Phys. Rev.* E **74** 11201
[38] Zaccarelli E, Foffi G, Dawson K A, Buldyrev S V, Sciortino F and Tartaglia P 2003 *J. Phys.: Condens. Matter* **15** S367
[39] Hansen J P and McDonald I R 1986 *Theory of Simple Liquids* (New York: Academic)
[40] Ng K C 1974 *J. Chem. Phys.* **61** 2680
[41] Rogers F J and Young D A 1984 *Phys. Rev.* A **30** 999
[42] Lang A, Kahl G, Likos C N, Löwen H and Watzlawek M 1999 *J. Phys.: Condens. Matter* **11** 10143
[43] Allen M P and Tildesley D J 1987 *Computer Simulation of Liquid* (New York: Clarendon)
[44] Frenkel D and Smit B 2002 *Understanding Molecular Simulation: From Algorithms to Applications* (San Diego, CA: Academic)
[45] Panagiotopoulos A Z 1987 *Mol. Phys.* **61** 813
[46] Smit B, de Smedt P H and Frenkel D 1989 *Mol. Phys.* **68** 931
[47] Gil-Villegas A, Vega C, del Río F and Malijevsky A 1995 *Mol. Phys.* **86** 857
[48] Liu Y, Chen W R and Chen S H 2005 *J. Chem. Phys.* **122** 044507
[49] Broccio M, Costa D, Liu Y and Chen S H 2006 *J. Chem. Phys.* **124** 084501
[50] Hansen J P and Verlet L 1969 *Phys. Rev.* **184** 151
[51] Puertas A M, Fuchs M and Cates M E 2002 *Phys. Rev. Lett.* **88** 98301
[52] Puertas A M, Fuchs M and Cates M E 2003 *Phys. Rev.* E **67** 31406
[53] Cates M E, Fuchs M, Kroy K, Poon W C and Puertas A M 2004 *J. Phys.: Condens. Matter* **16** S4861
[54] Yeomans-Reyna L, Acuña-Campa H and Medina-Noyola M 2000 *Phys. Rev.* E **62** 3395
[55] Yeomans-Reyna L and Medina-Noyola M 2001 *Phys. Rev.* E **64** 66114
[56] Chávez-Rojo M A and Medina-Noyola M 2005 *Phys. Rev.* E **72** 31107